

Article

Preparation of High-Purity Magnesium from Electrolytically Produced Crude Magnesium via Vacuum Distillation

Zhanshan Ma ^{1,*}, Shangrun Ma ², Fuxing Zhu ^{1,*}, Kaihua Li ¹, Zhuo Sheng ¹, Zhanjun Li ¹ and Yaowu Wang ^{3,*}

¹ State Key Laboratory of Vanadium and Titanium Resources Comprehensive Utilization, Pangang Group Research Institute Co., Ltd., Panzhihua 617000, China

² National Engineering Laboratory for Vacuum Metallurgy, Kunming University of Science and Technology, Kunming 650093, China

³ College of Metallurgy, Northeastern University, Shenyang 110819, China

* Correspondence: mazhanshan2023@163.com (Z.M.); zhufuxing@stu.cdu.edu.cn (F.Z.); wangyw@smm.neu.edu.cn (Y.W.); Tel.: +86-028-338-0581 (F.Z.)

Abstract: Metallic Mg is an important strategic metal and its properties are greatly affected by impurities. Silico-thermic reduction and electrolysis are the most used approaches to prepare metallic Mg. The products of these processes need to be further refined to obtain high-purity Mg metal. However, previous research has mainly focused on refining the crude Mg (CM) produced via silico-thermic reduction, whereas no in-depth investigations have been conducted on refining the CM produced via electrolysis. Here, vacuum distillation was used to refine electrolytically produced CM. The content and morphological characteristics of the impurity elements in CM were studied via glow discharge mass spectrometry, mineral dissociation analysis, and electron probe microanalysis. The effect of different distillation temperatures and times on the quality of the refined Mg was investigated. The results show that the main impurity elements are Al, Fe, Si, Ti, Cr, S, Cl, and Ni. The content of impurities, such as Si, Al, Fe, Ni, Ti, and Cr, in the refined Mg is significantly reduced at a temperature of 1023 K and a time of 120 min, and the purity of the refined Mg reaches 99.99%, which meets the Mg9999 national standard for primary Mg ingots in China (GB/3499-2011).



Citation: Ma, Z.; Ma, S.; Zhu, F.; Li, K.; Sheng, Z.; Li, Z.; Wang, Y. Preparation of High-Purity Magnesium from Electrolytically Produced Crude Magnesium via Vacuum Distillation. *Metals* **2023**, *13*, 811. <https://doi.org/10.3390/met13040811>

Academic Editor: Antoni Roca

Received: 28 February 2023

Revised: 8 April 2023

Accepted: 18 April 2023

Published: 20 April 2023



Copyright: © 2023 by the authors. Licensee MDPI, Basel, Switzerland. This article is an open access article distributed under the terms and conditions of the Creative Commons Attribution (CC BY) license (<https://creativecommons.org/licenses/by/4.0/>).

1. Introduction

Metallic Mg is a light metal with active chemical properties, possessing the advantages of a low density [1], a high electromagnetic shielding ability [2], and a good thermal fatigue performance [3]. Thus, it is not only widely used in the automotive, electronics, aerospace, and steel industries, but also as a reducing agent for the preparation of metallic titanium, zirconium, and uranium [4–12]. Thermal reduction and electrolysis are the two main methods used to produce metallic Mg. Thermal reduction consists of reducing MgO to Mg metal through the use of reducing agents, such as ferrosilicon and graphite, in vacuum at high temperature [13,14]. The electrolytic process consists of the electrochemical reduction of MgCl₂ to metallic Mg in a molten salt system [15]. Currently, metallic Mg is mainly produced through the silico-thermic reduction process (Pidgeon process) in industry. The electrolytic process is mainly used for the realization of the entire “Mg–Cl” cycle and the clean production of sponge titanium [16–25]. The electrolysis of MgO was conducted using a liquid tin (Sn) cathode and a carbon (C) anode in the eutectic composition of a magnesium fluoride (MgF₂)—lithium fluoride (LiF) molten salt to produce high-purity Mg [25]. The distinct morphological formation of Mg in different condensed form is probably attributed to the differences in surface energy change of Mg during the condensation process [26].

Regardless of whether metallic Mg is produced via silico-thermic reduction or electrolysis, it contains a certain number of impurities and thus requires refining. According to the

different refining methods, the Mg refining process can be broadly classified into solvent refining and vacuum distillation refining. Solvent refining is a method to remove impurities in crude Mg (CM) by adding a certain amount of a refining agent in a crucible furnace or a continuous refining furnace. It is the main method for refining Mg utilized in industries at present. However, due to the influence of the impurity elements and the refining co-solvent, this method has limited ability to remove impurities from the refined Mg and cannot directly produce high-purity Mg [27–30]. Vacuum distillation [31–35] refining can be used to obtain high-purity Mg by exploiting the difference in the vapor pressure between impurities and metallic Mg; this method has received considerable attention in recent years. It has already been reported that high-purity Mg can be obtained from CM produced via silicothermic reduction using vacuum distillation refining. However, due to the large difference in the CM quality obtained via silicothermic reduction and the electrolytic process, the effect of vacuum distillation on the refining of the electrolytically produced CM is not yet clear. Therefore, this study presents a novel process based on vacuum distillation for preparing high-purity Mg from electrolytically produced CM. The state of the impurities in CM and their separation during the vacuum distillation process are thoroughly studied via glow discharge mass spectrometry (GD-MS), electron probe microanalysis (EPMA), and mineral dissociation analysis (MLA) [34–37]. The results show that the content of impurities, such as Si, Al, Fe, Ni, Ti, and Cr, in the refined Mg is significantly reduced at a distillation temperature of 1023 K and a distillation time of 120 min, and the purity of the refined Mg can reach 99.99%.

2. Theoretical Equilibrium Vapor Pressure of Vacuum Distillation

The separation of different components using vacuum distillation is based on the equilibrium vapor pressure of different substances. At a given system pressure, components with a higher vapor pressure will be more easily volatilized and separated from the raw material upon increasing the temperature. The equilibrium vapor pressure of a pure substance as a function of temperature can be expressed as follows [38]:

$$\lg p^* = AT^{-1} + B \lg T + CT + D, \quad (1)$$

where p^* refers to the saturation vapor pressure of a pure substance (in Pa); T denotes the temperature (in K); A , B , C , and D are evaporation constants.

The order in which impurities are volatilized during the distillation process depends on their saturation vapor pressure, i.e., substances with a high vapor pressure tend to volatilize before those with a low vapor pressure. The relationship between the saturation vapor pressure and temperature for different metals is shown in Figure 1. The degree of separation between each impurity and magnesium is different. We calculated the saturated vapor pressure of nine impurities at 900, 923, 973, and 1073 K using Equation (1). As shown in Figure 1, the saturation vapor pressure of impurities in magnesium is considerably different. At temperatures of 900, 923, 973, and 1073 K, the saturated vapor pressure of Na and K is the largest, which is very close to magnesium, only one order of magnitude away, while the three elements are the first to evaporate. As temperature rises, Li, Ca, Pb, and Mn subsequently evaporate. The remaining Fe and Al have very low vapor pressure and are not volatile. Therefore, the evaporation mass of these elements is relatively small.

Generally, CM contains several impurities, such as Al, Mn, Fe, Na, K, Ca, and Pb. However, the CM produced via electrolysis usually contains mainly Fe, Al, Ti, and Cl, while that produced via the Pidgeon process contains mainly Al, Mn, Si, and Zn. Vacuum distillation refining requires that the boiling points of Na, K, and Zn are lower than that of Mg, and that the boiling points of Al, Mn, Fe, Ni, Cu, Pb, and Si are significantly higher than that of Mg. This allows Mg to evaporate, leaving behind the above elements, which can be separated more accurately due to the different boiling points [39].

The vapor pressure p_i of group element i in the crude metal is different from the vapor pressure p_i^* when i is a pure substance; this is the result of molecular interactions with

other impurity elements as well as the difference in concentration. Thus, the vapor pressure of group element i can be calculated as [40]:

$$p_i = a_i p_i^* = \gamma_i x_i p_i^*, \quad (2)$$

where p_i is the vapor pressure of group element i (in Pa); a_i is the activity of group element i ; p_i^* is the vapor pressure of group element i in the case this is a pure substance (in Pa); γ_i is the activity coefficient of group element i ; x_i is the concentration of group element i .

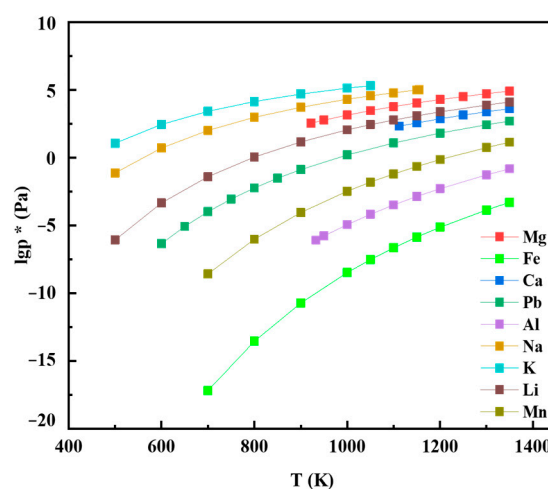


Figure 1. Relationship between the saturation vapor pressure and temperature for different metals.

The vapor density ρ_i can be calculated as [41]:

$$\rho_i = \frac{x_i \gamma_i M_i p_i^*}{RT}, \quad (3)$$

where ρ_i is the vapor density of group element i (in g/cm³); M_i is the molar mass of group element i (in g/mol); R is the molar gas constant (in J·mol⁻¹ K⁻¹); T is the temperature (in K).

The ratio between A and B can be calculated according to:

$$\rho_A / \rho_B = \frac{x_A \gamma_A M_A p_A^*}{x_B \gamma_B M_B p_B^*}, \quad (4)$$

where ρ_A and ρ_B are the vacuum densities of group elements A and B , respectively (in g/cm³); x_A and x_B are the concentrations of group elements A and B , respectively; γ_A and γ_B are the activity coefficients of group elements A and B , respectively; M_A and M_B are the relative atomic masses of group elements A and B , respectively; p_A^* and p_B^* are the vapor pressures of group elements A and B , respectively (in Pa).

The molar fraction ratio of components A and B with mass fractions a and b , respectively, (corresponding to mole fractions x_A and x_B , respectively) can be also calculated using Equation (4), which yields:

$$\frac{x_A}{x_B} = \frac{a M_B}{b M_A}. \quad (5)$$

When the molecular structure of the gas–liquid phase is the same, Equation (5) can be simplified to:

$$\frac{\rho_A}{\rho_B} = \frac{a}{b} \cdot \frac{\gamma_A}{\gamma_B} \cdot \frac{p_A^*}{p_B^*}. \quad (6)$$

The value of β_A in Equation (6) can be calculated as:

$$\beta_A = \frac{\gamma_A}{\gamma_B} \cdot \frac{p_A^*}{p_B^*}. \quad (7)$$

Therefore, the ratio of the vapor pressure of components A and B can be calculated as:

$$\frac{\rho_A}{\rho_B} = \beta_A \frac{a}{b}. \quad (8)$$

The left-hand side of Equation (8) is the ratio of the two components in the gas phase, whereas the right-hand side is the ratio of the two components in the condensed phase. β_A is called the separation coefficient and indicates the difficulty of separating component A from component B. When $\beta_A > 1$, component A is more concentrated in the gas phase, component A evaporates in preference to component B, and components A and B can be easily separated. When $\beta_A < 1$, component A is more concentrated in the liquid phase, component B evaporates in preference to component A, and components A and B can still be easily separated. When $\beta_A = 1$, it is difficult to separate components A and B.

3. Experimental Procedures

3.1. Sample Preparation

CM was obtained via multipole Mg electrolysis (Pangang Group Titanium Metal Materials Co., Ltd., Panzhihua, China), which was electrochemically reduced from $MgCl_2$, a by-product of the titanium sponge production, in $NaCl-CaCl_2-MgCl_2-CaF_2$ melts at around 660 °C. The electrolysis process parameters have been reported in a previous work [42–44]. The sampling spoon was first used to pour the molten Mg on the surface of the electrolyzer into the iron crucible, and after natural cooling, the cooled Mg ingots were reacted with hydrochloric acid (concentration of 5–10%) for 30 min to remove the oxide film on the surface; the surface was then washed with deionized water to remove the hydrochloric acid. Subsequently, the obtained Mg ingot samples were dried in an oven at 60 °C for 12 h. The photographs of the obtained CM samples are shown in Figure 2a. Figure 2b shows the magnesium chips obtained by drilling machine processing of crude magnesium samples before distillation, which are used for impurity content detection and analysis. CM samples are shown in Figure 2c. The samples were cut into squares with a side length of 2.5 cm and a height of 1 cm using a wire cutter (DK350, Guangdong Datie, China), and then their surfaces were polished using 1000-grit sandpaper and wiped with acetone to remove possible stains.

3.2. Vacuum Distillation Experiments

Firstly, approximately 200 g of the above Mg ingots were placed into high-purity Mg oxide crucibles with diameter and height of 300 and 100 mm, respectively. Then, the MgO crucible was transferred to a vacuum distillation furnace (Shenyang Vacuum Technology Research Institute). The maximum heating power, maximum temperature, and ultimate vacuum of the distillation furnace were 5 kW, 1473 K, and 5×10^{-3} Pa, respectively. When the pressure of the system reached 5 Pa, the heating power was turned on and the temperature was increased at a rate of 5 K s^{-1} to investigate the effects of the distillation temperature, distillation time, and ultimate vacuum on the quality of the distilled products. The condenser is made of quartz material with diameter and length of 150 and 300 mm respectively. The inside of the condenser is lined with high purity graphite foil, whose thickness is 0.2 mm and has good flexibility. The high purity magnesium is eventually condensed on the high purity graphite foil, which is very easy to separate from the condenser and will not react with the high purity magnesium. After the distillation was completed, the heating system was turned off, and the vacuum pump was then run continuously until the furnace temperature cooled to room temperature. Finally, argon gas was flushed in, and the condensed product and distillation residue were removed for

weighing and sample analysis. A schematic of the vacuum distillation unit is shown in Figure 3.

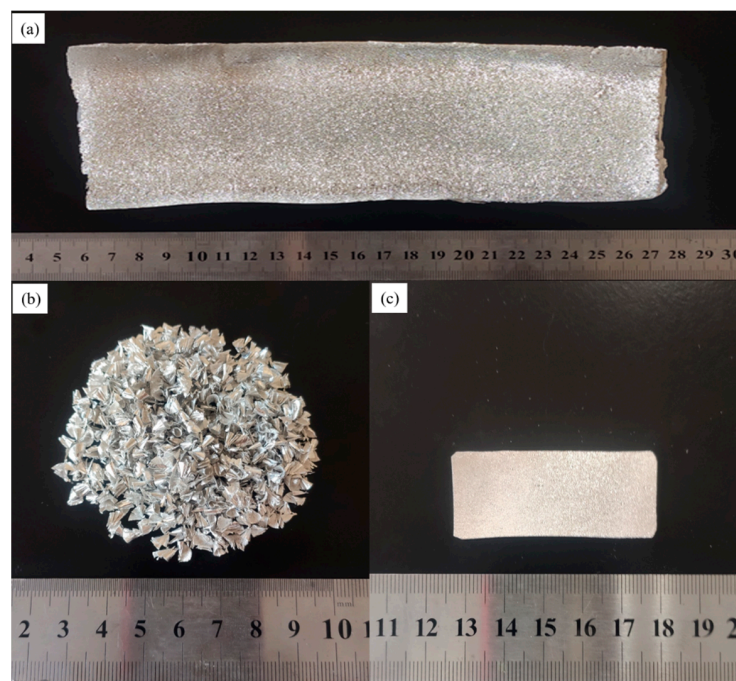


Figure 2. Photographs of (a) the electrolytically produced CM product, (b) the Mg scrap, and (c) the Mg block.

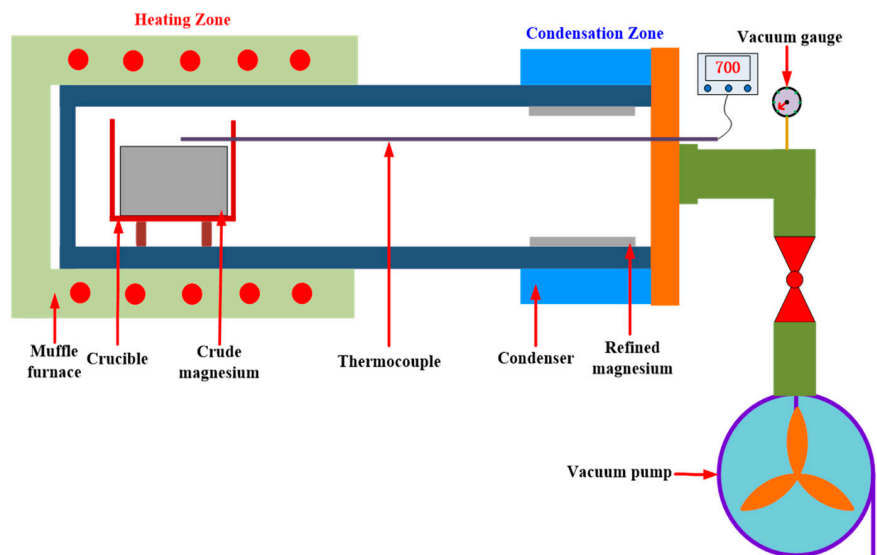


Figure 3. Schematic of the vacuum distillation device.

The volatilization yield E_v of metallic Mg during distillation was calculated as:

$$E_v = \frac{M_1 - M_2}{M_1} \times 100\%, \quad (9)$$

where M_1 is the mass of the raw material (in g), and M_2 is the mass of the residue (in g).

3.3. Sample Characterization

The composition of the samples was analyzed via GD-MS (Astrum ES, NU, Wrexham, UK). Additionally, the state and morphological characteristics of the impurity elements on

the surface of the CM samples were analyzed via EPMA (JXA-IHP200F, JEOL, Tokyo, Japan) and MLA (MLA-250, FEI Czech Co., Ltd., Hillsboro, OR, USA). The physical phase of the distillation residue was analyzed via X-ray diffraction (XRD, XRD-7000, Shimadzu, Japan) using a cobalt target at an electron gun voltage and current of 35 V and 20 kA, respectively.

4. Results and Discussion

4.1. State of the Impurities in CM

The contents of the impurities in CM are listed in Table 1. It can be seen that the main impurities in the CM products are Al, Fe, Si, Ti, Cr, S, Cl, Na, and Ni. The Al and Fe contents are 0.0243% and 0.0184%, respectively. According to the original magnesium ingot GB/T 3499-2011 released by Standards Committee of China, the content of Al element in 9999 grade Mg is less than or equal to 20 ppm, the content of Fe element is less than or equal to 20 ppm, and the content of Ti element is less than or equal to 5 ppm. Fe, Al, and Ti are the main removal objects in this experiment.

Table 1. Typical impurity content in the CM products determined via GD-MS.

Category	Al/%	Fe/%	Si/%	Ti/%	Cr/%	S/%	Cl/%	Na/%	Ni/%
Electrolytic process	0.0243	0.0184	0.0072	0.0061	0.0015	0.0026	0.0106	0.0013	0.0011
Mg9999 [15]	0.002	0.002	0.002	0.0005	-	-	-	-	0.0003

To further analyze the state of the existing impurities, the electrolytically produced CM was characterized via MLA, and the corresponding results are shown in Figure 4. It can be seen from Figure 4 that the impurities in CM are not uniformly distributed, and there are local inclusions. The most important inclusions consist of MgO, which also represents the main form of the O impurities. The Al and Si impurities mainly exist in CM in the form of silicate. The impurity elements Al and Si are mainly derived from the electrolytic cell of the production unit of magnesium electrolytic system, which is made of firebrick, and the main raw material of firebrick is made of silicate. Ti impurities mainly come from titanium particles produced in the reduction distillation process of sponge titanium. In the reduction process, MgCl₂ needs to be discharged from the reduction tank and transported to the electrolytic unit by rail car. MgCl₂ is used as the raw material of magnesium electrolytic system. Therefore, titanium sponge inevitably appears in the electrolytic CM, which mainly exists in the form of TiN and Ti. The impurity content of Fe and Cr in the electrolytic CM is low, which mainly comes from the steel reactor of the electrolytic system and mainly exists in the form of alloy phase.

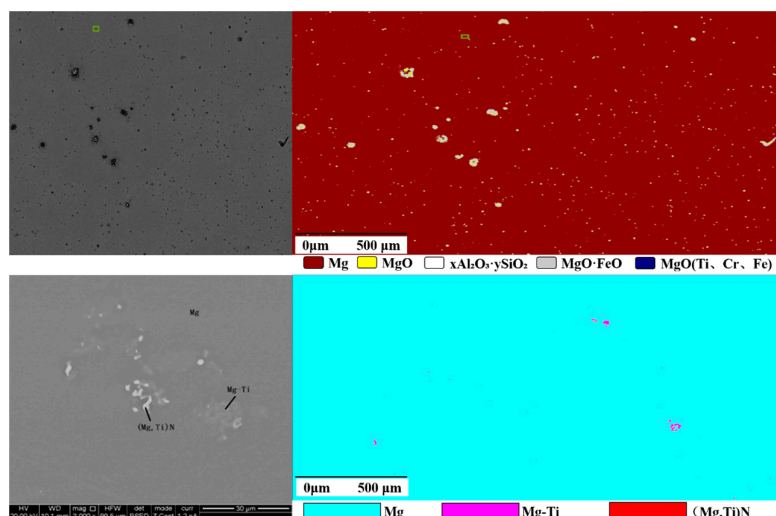


Figure 4. MLA results for the electrolytically produced CM.

In order to further analyze the presence of impurities, an electron probe was used to characterize the CM generated by electrolysis, and the results are shown in Figure 5. The EPMA results in Figure 5 show that the relative contents of Ti, Fe, Al, and Si of the inclusions in CM were higher, and the spots of relatively high concentrations of Ti, Fe, Al, and Si match each other quite well but not with that for oxygen. Consequently, these elements did not form inclusions that consist of silicates but of metallic phases, which is consistent with the MLA results. Moreover, the content of other impurity elements in electrolytic CM is low.

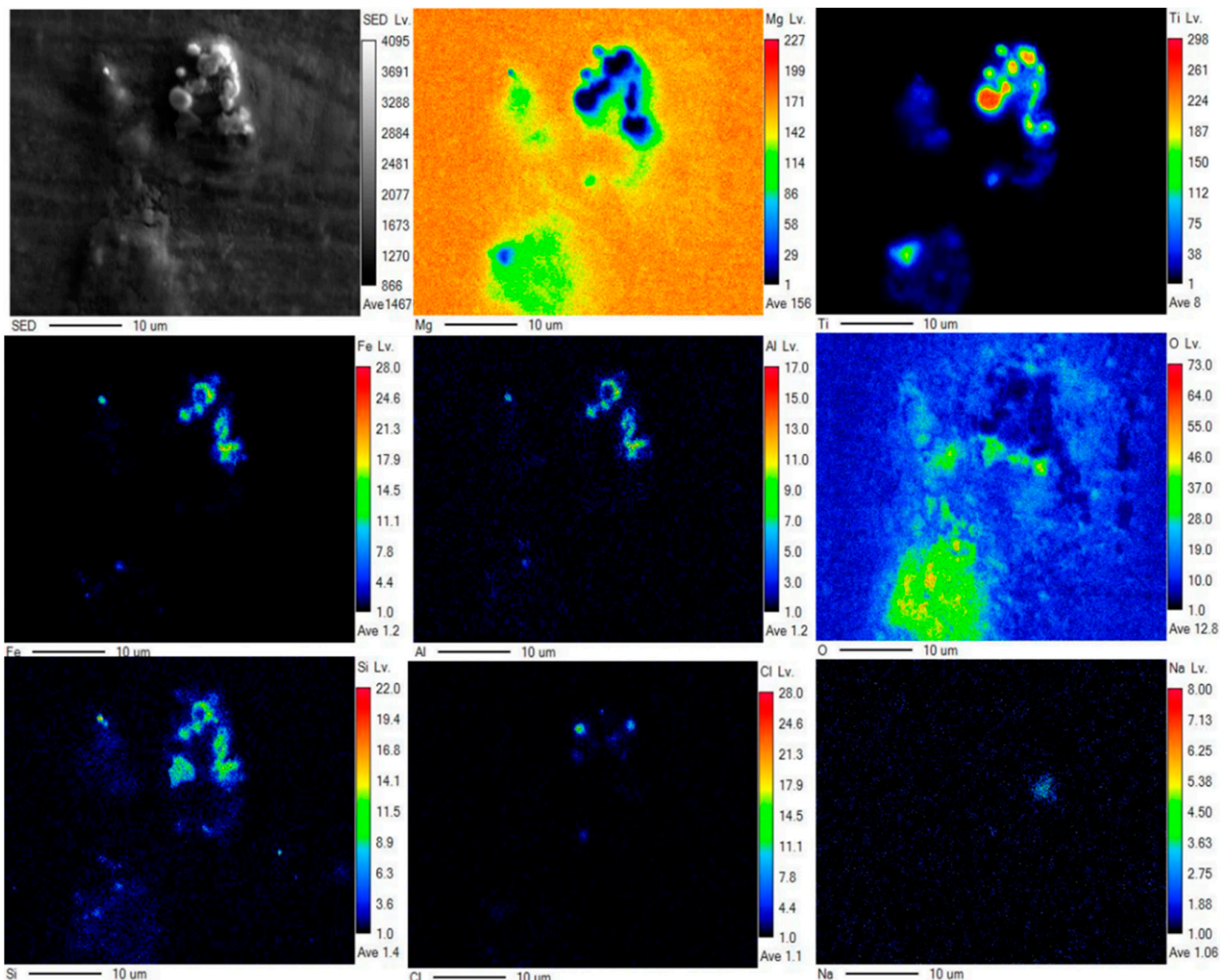


Figure 5. EPMA results for the electrolytically produced CM.

According to the corresponding vapor pressure of each element, the separation coefficient β of Mg from the impurities at different temperatures can be calculated, and the results are provided in Table 2. It can be seen that the separation coefficient β is less than 1 for the main impurity elements, such as Al, Fe, Mn, and Ni, in electrolytically produced CM, indicating that metallic Mg and the impurity elements can be easily separated. The activity coefficient γ of each component is 1 because the CM can be regarded as an infinite dilute solution with 7 impurities such as Pb, and Mn, as the solutes. This shows that Pb, Mn, Al, Fe, Ni, and Si have significant tendency to be separated from Mg but also different separation behaviors owing to the different β coefficients. However, the β coefficients of K and Na are always greater than one, denoting that K and Na are mainly concentrated in

the gas phase. During the entire distillation process, K and Na evaporate first, followed by Mg, which is enriched in the gas phase. As the distillation temperature increases, the electrolytically produced CM melts first. During the melting process, both K, Na, and Mg evaporate. At this time, there are many impurities in the magnesium melt. High melting and boiling point impurities, such as Pb, Mn, Al, Fe, Ni, and Si are not easy to evaporate. Such impurities get concentrated in the incompletely evaporated magnesium liquid and remain at the bottom of the crucible after the distillation is completed. Some impurities may evaporate and finally condense and collect in the condenser along with the magnesium vapor. In addition, impurities, such as MgO and TiN, have a very low saturated vapor pressure, which is beneficial to their vacuum distillation separation and removal.

Table 2. Separation coefficients of Mg and the various impurities at different temperatures.

T/K	β (Pb)	β (Mn)	β (Al)	β (Cu)	β (Fe)	β (Ni)	β (Si)
973	8.74×10^{-4}	1.38×10^{-6}	4.25×10^{-9}	3.96×10^{-10}	9.36×10^{-13}	5.47×10^{-14}	3.97×10^{-15}
1023 [44]	1.35×10^{-3}	3.53×10^{-6}	1.35×10^{-8}	1.49×10^{-9}	4.84×10^{-12}	3.54×10^{-13}	2.96×10^{-14}

4.2. Influence of the Distillation Process on the Quality of the Refined Mg

To determine the optimal distillation temperature and time, the influence of the distillation temperature and time on the volatilization rate of metallic Mg and the removal of the impurities were studied according to the parameters listed in Table 3, and the corresponding experimental results are shown in Figure 6.

Table 3. Vacuum distillation parameters used for the different tests.

No.	Temperature/K	Holding Time/min	Pre-Distillation Mass/g	Condensed Mg Mass/g	Residual/g	Post-Distillation Pressure/Pa
1	900	60	203.5	61.46	142.04	8.5
2	900	90	206.4	71.41	134.99	7.5
3	900	120	203.1	88.75	114.35	6.3
4	900	180	206.3	107.89	98.41	5.6
5	923	60	210.5	86.52	123.98	4.8
6	923	90	198.3	125.92	72.38	3.2
7	923	120	205.9	162.25	43.65	2.5
8	923	180	207.2	183.58	23.62	2.0
9	973	30	196.3	72.43	123.87	1.9
10	973	60	198.3	157.25	41.05	1.5
11	973	90	204.1	198.18	5.92	1.3
12	973	120	206.8	203.70	3.10	1.3
13	1023	30	201.3	111.92	89.38	1.7
14	1023	60	195.6	165.28	30.32	1.4
15	1023	90	206.3	202.79	3.51	1.3
16	1023	120	204.7	202.65	2.05	1.3

It can be seen in Figure 6a that with increasing distillation time, CM was not distilled completely, and the highest evaporation rate was only 52.3% at 900 K. It is obviously not meaningful to continue to extend the holding time at 900 K. However, as the distillation temperature reached 923 K, CM could be collected on the condenser after vacuum distillation, and the evaporation yield reached 88.6%. Obviously, the evaporation yield at 923 K still has a lot of room to improve. As the distillation temperature reached 1023 K, upon increasing the distillation time from 30 to 120 min, the evaporation yield increased from 55.6% to 99.0%. At temperatures of 973 and 1023 K, respectively, holding time more than 90 min, the evaporation yield reached above 90%.

It can be seen in Figure 6b that for a given distillation time and with increasing distillation temperature, the separation of the Al, Fe, Cl, and Si impurities with a lower

vapor pressure is more effective than that of the Ti, Cr, and Ni impurities; as the temperature increases from 900 to 1023 K, the content of the Al, Fe, Cl, and Si impurities decreases from 0.0138%, 0.0124%, 0.0098%, and 0.0069% to 0.0011%, 0.0009%, 0.0007%, and 0.0009%, respectively. It is noted that the contents of the Ti, Cr, S, Na, and Ni impurities in CM are reduced to different extents. Therefore, the distillation temperature of 1023 K and the distillation time of 120 min were chosen as the optimal conditions for the preparation of refined Mg via vacuum distillation.

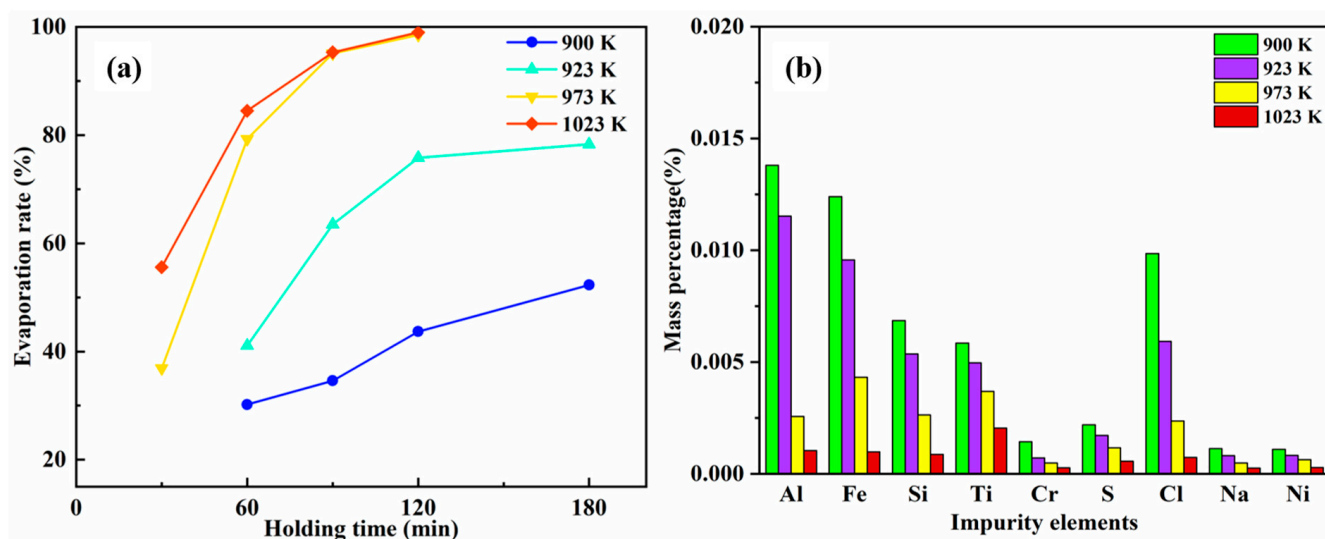


Figure 6. Effect of the distillation temperature and time on (a) the evaporation yield of Mg and (b) the removal of the impurity elements.

Table 4 shows the impurity content of metal magnesium after distillation. The electrolytically produced CM reached the 4N national standard via distillation, and the high contents of Al, Fe, Si, and Na impurities in the raw materials were all reduced below the standard line. The remaining impurities (Ni, Cr, and Ti) that reached the standard did not change significantly with the distillation temperature.

Table 4. Content of the impurities in Mg metal after distillation.

Temperature/K	Al	Fe	Si	Ti	Cr	S	Cl	Na	Ni
900	0.0138	0.0124	0.0069	0.0058	0.0014	0.0022	0.0098	0.0011	0.0011
923	0.0115	0.0096	0.0054	0.0049	0.0007	0.0018	0.0059	0.0008	0.0008
973	0.0026	0.0043	0.0026	0.0037	0.0005	0.0012	0.0024	0.0005	0.0006
1023	0.0011	0.0009	0.0009	0.0021	0.0003	0.0005	0.0007	0.0002	0.0003

Figure 7 shows the photographs of the high-purity Mg obtained via distillation and the residue in the crucible alongside their respective XRD patterns. Figure 7a,d show that high-purity Mg can be collected on the condenser at a distillation temperature of 1023 K and a distillation time of 120 min. After distillation, approximately 2 g MgO can be collected from electrolytic CM sample. Due to its very low saturated vapor pressure and high melting point, colorless solid MgO impurities are finally collected on the MgO crucible. Figure 7b shows the MgO photos obtained after distillation, and Figure 7c shows the XRD test results of high purity magnesium obtained after electrolytic CM distillation. The effective and efficient removal of MgO impurity and the refining of Mg were realized.

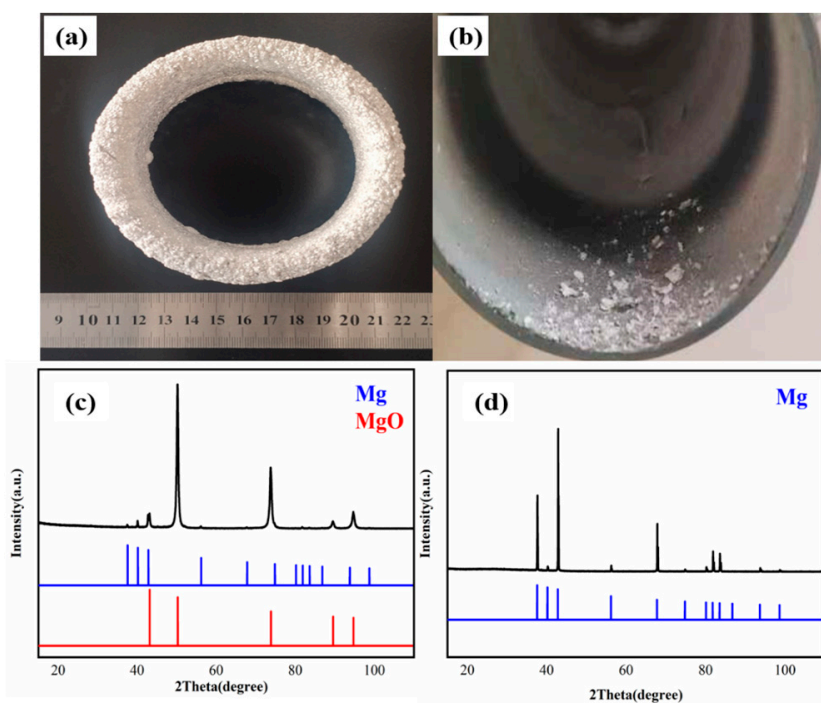


Figure 7. (a) Photograph of the distilled Mg collected on the condenser, (b) photograph of the residue after Mg distillation, (c) XRD patterns of the CM before distillation, and (d) XRD patterns of the distilled substance.

5. Conclusions

In this study, the state of the impurities in electrolytically produced CM as well as the preparation process of high-purity Mg metal via vacuum distillation were systematically studied through GD-MS, EPMA, MLA, and XRD. The results show that the Al, Fe, Si, Ti, Cr, S, Cl, Na, and Ni elements are the main impurities in electrolytically produced CM, which exhibit an uneven distribution and local inclusions. During the vacuum distillation process, the content of the Al, Fe, and Si impurities is drastically reduced, while that of other impurities, such as Ti, Cr, S, Na, and Ni, decreases by a different amount. Refined Mg with 99.99% purity can be collected on the condenser at a distillation temperature of 1023 K and a distillation time of 120 min; this high purity degree meets the Mg9999 national standard for primary Mg ingots in China (GB/3499-2011).

Author Contributions: Conceptualization, Z.M. and S.M.; methodology, Z.M.; validation, Z.M., F.Z., and K.L.; formal analysis, Z.M. and S.M.; investigation, Z.M. and Z.L.; resources, Y.W.; data curation, Z.M. and Z.S.; writing—original draft preparation, Z.M.; writing—review and editing, F.Z. and Y.W.; visualization, Z.M. and S.M.; supervision, F.Z. and Y.W.; project administration, Z.M.; funding acquisition, Z.M. All authors have read and agreed to the published version of the manuscript.

Funding: The research presented in this work was funded by the Orientation Development Plan of Sichuan Province, China (2017GZYZF0039).

Data Availability Statement: The data is available to contact the author (wangyw@smm.neu.edu.cn).

Acknowledgments: This work was supported by the Orientation Development Plan of Sichuan Province, China (2017GZYZF0039).

Conflicts of Interest: The authors declare no conflict of interest.

References

1. Froes, F.H.; Eliezer, D.; Aghion, E. The science, technology, and applications of magnesium. *JOM* **1998**, *50*, 30–34. [CrossRef]
2. Song, K.; Pan, F.S.; Chen, X.H.; Zhang, Z.H.; Tang, A.T.; She, J.; Yu, Z.W.; Pan, H.C.; Xu, X.Y. Effect of texture on the electromagnetic shielding property of magnesium alloy. *Mater. Lett.* **2015**, *157*, 73–76. [CrossRef]

3. Li, S.; Yang, X.; Hou, J.; Du, W. A review on thermal conductivity of magnesium and its alloys. *J. Magnes. Alloy.* **2020**, *8*, 78–90. [[CrossRef](#)]
4. Gray, J.E.; Luan, B. Protective coatings on magnesium and its alloys—A critical review. *J. Alloys Compd.* **2002**, *336*, 88–113. [[CrossRef](#)]
5. Figueiredo, R.B.; Poggiali, F.S.J.; Silva, C.L.P.; Cetlin, P.R.; Langdon, T.G. The influence of grain size and strain rate on the mechanical behavior of pure magnesium. *J. Mater. Sci.* **2015**, *51*, 3013–3024. [[CrossRef](#)]
6. Somekawa, H.; Mukai, T. Hall–Petch breakdown in fine-grained pure magnesium at low strain rates *Mater. Trans. A* **2014**, *46*, 894–902. [[CrossRef](#)]
7. Kulekci, M.K. Magnesium and its alloys applications in automotive industry. *Int. J. Adv. Manuf. Tech.* **2007**, *39*, 851–865. [[CrossRef](#)]
8. You, S.; Huang, Y.; Kainer, K.U.; Hort, N. Recent research and developments on wrought magnesium alloys. *J. Magnes. Alloy.* **2017**, *5*, 239–253. [[CrossRef](#)]
9. Pan, F.; Yang, M.; Chen, X. A Review on casting magnesium alloys: Modification of commercial alloys and development of new Alloys. *J. Mater. Sci. Technol.* **2016**, *32*, 1211–1221. [[CrossRef](#)]
10. Xia, X.; Chen, X.; Zhao, W.; Xue, H.; Liao, B.; Hur, B.; Wang, Z. Corrosion behavior of closed-cell AZ31 Mg alloy foam in NaCl aqueous solutions. *Corros. Sci.* **2014**, *80*, 247–256. [[CrossRef](#)]
11. Luo, A.A. Recent magnesium alloy development for elevated temperature applications. *Int. Mater. Rev.* **2004**, *49*, 13–30. [[CrossRef](#)]
12. Hort, N.; Huang, Y.; Kainer, K.U. Intermetallics in magnesium alloys. *Adv. Eng. Mater.* **2006**, *8*, 235–240. [[CrossRef](#)]
13. Wulandari, W.; Brooks, G.; Rhamdhani, M.; Monaghan, B. Magnesium: Current and Alternative Production Routes. In *Australian Conference on Chemical Engineering*; University of Wollongong Australia: Wollongong, Australia, 2010.
14. Pekguleryuz, M.; Mackenzie, L. (Eds.) Pilot Plant Demonstration of the Mintek Thermal Magnesium Process. In Proceedings of the Conference of Metallurgists, Montréal, QC, Canada, 1–4 October 2006.
15. GB/T 3499-2011; Standard of the People's Republic of China for Primary Magnesium Ingots. The Chinese Standards Committee: Beijing, China, 2011.
16. Birbilis, N.; King, A.; Thomas, S.; Frankel, G.S.; Scully, J.R. Evidence for enhanced catalytic activity of magnesium arising from anodic dissolution. *Electrochim. Acta* **2014**, *132*, 277–283. [[CrossRef](#)]
17. Duhaime, P.; Mercille, P.; Pineau, M. Electrolytic process technologies for the production of primary magnesium. *Miner. Process Extr. Metall. Rev.* **2002**, *111*, 53–55. [[CrossRef](#)]
18. Du, J.; Han, W.; Peng, Y. Life cycle greenhouse gases, energy and cost assessment of automobiles using magnesium from Chinese Pidgeon process. *J. Clean Prod.* **2010**, *18*, 112–119. [[CrossRef](#)]
19. Tian, Y.; Wang, L.; Yang, B.; Dai, Y.; Xu, B.; Wang, F.; Xiong, N. Comparative evaluation of energy and resource consumption for vacuum carbothermal reduction and Pidgeon process used in magnesium production. *J. Magnes. Alloy.* **2020**, *10*, 697–706. [[CrossRef](#)]
20. Mohamed, S.R.; Friedrich, S.; Friedrich, B. Refining principles and technical methodologies to produce ultra-pure magnesium for high-tech applications. *Metals* **2019**, *9*, 85. [[CrossRef](#)]
21. Inoue, M.; Iwai, M.; Matsuzawa, K.; Kamado, S.; Kojima, Y. Vacuum distillation refining and recycling of magnesium alloys. *Mater. Sci. Forum.* **2003**, *419–422*, 691–696. [[CrossRef](#)]
22. Bolivar, R.; Friedrich, B. Magnesiothermic reduction from titanium dioxide to produce titanium powder. *J. Sustain. Metall.* **2019**, *5*, 219–229. [[CrossRef](#)]
23. Choi, K.; Choi, H.; Sohn, I. Understanding the Magnesiothermic Reduction Mechanism of TiO₂ to Produce Ti. *Mater. Trans. B* **2017**, *48*, 922–932. [[CrossRef](#)]
24. Gao, F.; Nie, Z.; Yang, D.; Sun, B.; Liu, Y.; Gong, X.; Wang, Z. Environmental impacts analysis of titanium sponge production using Kroll process in China. *J. Clean. Prod.* **2018**, *174*, 771–779. [[CrossRef](#)]
25. Krauter, N.; Eckert, S.; Gundrum, T.; Stefani, F.; Wondrak, T.; Khalilov, R.; Dimov, I.; Frick, P. Experimental Validation of an Inductive System for Magnesium Level Detection in a Titanium Reduction Reactor. *Sensors* **2020**, *20*, 6798. [[CrossRef](#)] [[PubMed](#)]
26. Lee, T.H.; Okabe, T.H.; Lee, J.-Y.; Kim, Y.M.; Kang, J. Development of a novel electrolytic process for producing high-purity magnesium metal from magnesium oxide using a liquid tin cathode. *J. Magnes. Alloy.* **2021**, *9*, 1644–1655. [[CrossRef](#)]
27. Yang, B.; Liang, D.; Xiong, N.; Tian, Y.; Xu, B.; Dai, Y. Effect of crystallization on purity of volatile metallic magnesium prepared from a one-step multi-region condensation process under vacuum condition. *J. Magnes. Alloy.* **2022**, *10*, 3281–3287. [[CrossRef](#)]
28. Pan, F.S.; Chen, X.H.; Yan, T.; Liu, T.T.; Mao, J.J.; Luo, W.; Wang, Q.; Peng, J.; Tang, A.T.; Jiang, B. A novel approach to melt purification of magnesium alloys. *J. Magnes. Alloy.* **2016**, *4*, 8–14. [[CrossRef](#)]
29. Park, J.; Jung, Y.; Kusumah, P.; Dilasari, B.; Ku, H.; Kim, H.; Kwon, K.; Lee, C.K. Room temperature magnesium electrorefining by using non-aqueous electrolyte. *Met. Mater. Int.* **2016**, *22*, 907–914. [[CrossRef](#)]
30. Lee, J.H.; Nersisyan, H.; Huynh, T.N. Combustion-Alumino-Magnesiothermic Reduction of TiO₂ to Produce a Ti-Rich Ingots. *Mater. Sci. Forum.* **2022**, *53*, 3147–3158. [[CrossRef](#)]
31. Inoue, M.; Doi, T.; Aida, T.; Matsuki, K.; Kamado, S.; Kojima, Y. Vacuum distillation refining and extrusion process of magnesium. *Mater. Sci. Forum.* **2005**, *475–479*, 513–516. [[CrossRef](#)]
32. Lam, R.K.F.; Marx, D.R. Ultra High Purity Magnesium Vacuum Distillation Purification Method. U.S. Patent US 08/391,047, 10 December 1996.

33. Zhang, X.; Friedrich, S.; Bernd, F. Separation behavior of arsenic and lead from antimony during vacuum distillation and zone refining. *J. Mater. Res. Technol.* **2020**, *9*, 4386–4398. [[CrossRef](#)]
34. Revel, G.; Pastol, J.L.; Rouchaud, J.C.; Fromageau, R. Purification of Magnesium by Vacuum Distillation. *Metall. Mater. Trans. B* **1978**, *9*, 665–672. [[CrossRef](#)]
35. Papirov, I.I.; Kravchenko, A.I.; Mazin, A.I.; Shiyan, A.V.; Virich, V.D. Impurity distribution in a magnesium sublimate. *Inorg. Mater.* **2015**, *51*, 563–565. [[CrossRef](#)]
36. Mizuhara, K.; Inoue, M.; Aida, T.; Matsuzawa, K.; Aoyagi, N.; Miura, H. Preparation of ultra high purity magnesium sheet by vacuum distillation and extrusion. *Trans. GIGAKU* **2020**, *7*, 07004-1–07004-7. [[CrossRef](#)]
37. Rodushkin, I.; Ruth, T.; Huhtasaari, Å. Comparison of two digestion methods for elemental determinations in plant material by ICP techniques. *Anal. Chim. Acta* **1999**, *378*, 191–200. [[CrossRef](#)]
38. Mordike, B.L.; Ebert, T. Magnesium: Properties-applications-potential. *Mater. Sci. Eng. A* **2001**, *302*, 37–45. [[CrossRef](#)]
39. Han, J.B.; Fu, D.X.; Guo, J.H.; Ji, Z.H.; Dou, Z.H.; Zhang, T.A. Nucleation and Condensation of Magnesium Vapor in Argon Carrier. *Metals* **2020**, *10*, 1441. [[CrossRef](#)]
40. Wang, Y.C.; Tian, Y.; Qu, T.; Yang, B.; Dai, Y.; Sun, Y. Purification of Magnesium by Vacuum Distillation and its Analysis. *Mater. Sci. Forum* **2014**, *788*, 52–57. [[CrossRef](#)]
41. Yong, D.; Bin, Y. *Vacuum Metallurgy of Nonferrous Metal Materials*; Metallurgical Industry Press: Beijing, China, 2000.
42. Gesing, A.J.; Das, S.K. Use of Thermodynamic Modeling for Selection of Electrolyte for Electrorefining of Magnesium from Aluminum Alloy Melts. *Metall. Mater. Trans. B* **2017**, *48*, 132–145. [[CrossRef](#)]
43. Liu, C.L.; Zhao, Q.W.; Sun, Z. Analysis of Magnesium Droplets Characteristics and Separation Performance in a Magnesium Electrolysis Cell Based on Multiphysical Modeling. *Arab. J. Sci. Eng.* **2018**, *43*, 5965–5976. [[CrossRef](#)]
44. Tian, Y.; Zhang, X.P.; Qu, T.; Lyu, F.; Du, H.; Shi, L.; Yang, B.; Dai, Y.N. Technical research on vacuum distillation to purify magnesium to 99.99% purity. *Mater. Res. Express* **2021**, *8*, 056506. [[CrossRef](#)]

Disclaimer/Publisher's Note: The statements, opinions and data contained in all publications are solely those of the individual author(s) and contributor(s) and not of MDPI and/or the editor(s). MDPI and/or the editor(s) disclaim responsibility for any injury to people or property resulting from any ideas, methods, instructions or products referred to in the content.